

Analytical Models of Frequency and Voltage in Large-Scale All-Inverter Power Systems

Marena Trujillo^{*†‡}, Amir Sajadi^{†‡}, and Bri-Mathias Hodge^{*†‡}

^{*}Department of Electrical, Computer, and Energy Engineering, University of Colorado of Boulder, Boulder, Colorado 80309

[†]Renewable and Sustainable Energy Institute, University of Colorado of Boulder, Boulder, Colorado 80309

[‡]National Renewable Energy Laboratory, Golden, Colorado 80401

marena.trujillo@colorado.edu, amir.sajadi@colorado.edu, brimathias.hodge@colorado.edu

Abstract—Low-order frequency response models for power systems have a decades-long history in optimization and control problems such as unit commitment, economic dispatch, and wide-area control. With a few exceptions, these models are built upon the Newtonian mechanics of synchronous generators, assuming that the frequency dynamics across a system are approximately homogeneous, and assume the dynamics of nodal voltages for most operating conditions are negligible, and thus are not directly computed at all buses. As a result, the use of system frequency models results in the systematic underestimation of frequency minimum nadir and maximum RoCoF, and provides no insight into the reactive power-voltage dynamics. This paper proposes a low-order model of both frequency and voltage response in grid-forming inverter-dominated power systems. The proposed model accounts for spatial-temporal variations in frequency and voltage behavior across a system and as a result, demonstrates the heterogeneity of frequency response in future renewable power systems. Electromagnetic transient (EMT) simulations are used to validate the utility, accuracy, and computational efficiency of these models, setting the basis for them to serve as fast, scalable alternatives to EMT simulation, especially when dealing with very large-scale systems, for both planning and operational studies.

Index Terms—Frequency response, All-inverter systems, Low-inertia systems, Grid-forming inverters, Voltage dynamics

As the climate crisis drives extreme temperature changes, intensifying storms, and habitat destruction, the need for decarbonization is more urgent than ever. As a result, the adoption of wind, solar, and battery storage devices, which are power electronics-interfaced resources, continues to increase worldwide [1]. However, the physical principals determining the behavior of inverter-based resources (IBRs) are fundamentally different from that of conventional, synchronous machine-interfaced resources. As IBRs supplant synchronous generators (SGs), the dominant system dynamics shift from electromechanical modes to electromagnetic modes [2]. Thus, this transition from SGs to IBRs warrants new analytical models to best explain the underlying physical phenomena consistent with the nature of emerging power systems.

Analytical models are the building blocks of algorithms and the core engines behind all existing scientific and commercial simulation tools used in research and industry to predict the system behavior. However, there is always a trade-off between the granularity of results vs. the scale of system that can be simulated with reasonable computational effort. A review of the literature suggests that two general directions have emerged in modeling the dynamics of power systems.

The first direction focuses on different formulations, such as sinusoid waveform vs. phasor models. Sinusoid waveform models provide high-fidelity simulations of power systems by explicitly modeling all three phases and controllers, supporting the use of high-order, highly detailed device models, and having time step capabilities in the microsecond range [2]. However, solving waveform models, which is the engine in software packages such as Power System Computer Aided Design (PSCAD), remains impractical for use in large-scale systems due to their computational burden [2]. Alternatively, the use of phasor models, which are reduced-order models, utilize simplified device and network models and consequently their computational tractability is far superior to waveform models. However, while phasor models are attractive due to their computational tractability, they are less accurate than full-order models [2]. Positive sequence RMS (Root Mean Square) simulation tools, such as Power Systems Simulator for Engineers (PSSE) and PowerWorld, are examples of reduced-order models in the sense that they reduce a three-phase explicit model to a positive sequence model. However, these tools, which were developed based on the slow electromechanical dynamics of SGs are ill suited for modeling IBRs due to their large time steps (about 4 ms), and inability to model internal controllers [3]. While both the full-order models in EMT tools and the reduced-order models in positive sequence tools have clear shortcomings, there are also other methods of model reduction.

Order reduction can be achieved by eliminating non-dominant modes in the dynamics of variables of interest, and can be performed through various techniques, e.g., perturbation theory [4], integral manifolds [5], or simply through simplified physics-based reduction methods [6]. Almost universally, existing analytically reduced models for power systems are focused on system frequency (SFR) models, while developing such models for nodal voltage dynamics has not been a focus of the literature [6]–[14]. SFR models that aggregate the primary frequency response of a system take the order-reduction process to an extreme by omitting network effects and neglecting all variance in frequency response across a system [7]. SFR models have been widely used as a less computationally burdensome alternative to time domain simulation for the estimation of the frequency response of a system after a disturbance [6]–[14]. They yield reasonable approximations of

RoCoF and nadir frequency for SGs, which can then be formulated into constraints on frequency stability or under-frequency load-shedding in power systems optimization problems [8], [9]. In [6] and [7], lower-order SFR models are presented, but the SGs exhibit little heterogeneity in terms of governor and prime mover type. These models were intended to provide general information about a system’s frequency response post-disturbance [7], and to formulate margins that would ensure the minimum frequency following a disturbance would not be less than the load-shedding frequency threshold [6]. An open-loop model to calculate the maximum frequency deviation in a small isolated power system is proposed in [10]. This model allows for SGs with different governor, prime mover, and turbine characteristics, unlike the SFR model of [7]. In [11], a parabolic frequency deviation serves as the input to an open-loop SFR model to better predict system nadir. However, all of these models presume a SG-dominated system and most neglect the network dynamics and the spatial-temporal characteristics of frequency response. In all cases, reactive-power/voltage (Q-V) dynamics are completely disregarded.

IBR-rich systems typically feature power electronic devices with two prominent inverter control paradigms: grid-following inverters (GFLs) or grid-forming inverters (GFMs). Both devices provide power, but only GFMs construct frequency and regulate voltage independently. GFLs with grid support functionality, i.e. volt-var and volt-watt functions, can also manipulate frequency and voltage response through the regulation of active and reactive power, but they required a well-defined voltage waveform at their point of interconnection and they cannot independently form frequency [15]. For these reasons, we focus on GFMs in this work. With regards to the frequency response of inverters, the SFR model of [12] is intended to model systems with some amount of renewable generation, though all renewable generators are modeled as doubly fed induction generators with droop control. In [13], a nadir prediction model is proposed that accounts for three different types of fast frequency response provided by IBRs. However, the authors neglect the fast dynamics of IBRs and do not distinguish between GFL and GFM. The model in [14] omits inverter dynamics but makes the unique contribution of providing a closed-form solution of frequency response for a three SG system. In this work, a simplified network model is used to account for inter-machine frequency oscillations. However, application of [14] to large, multi-generator systems requires the aggregation of generators into three equivalent SGs. Importantly, the model presumes a flat voltage profile of 1pu across the system. The review of the literature on voltage models also reveals that existing reduced order models of GFM networks that account for voltage dynamics require the division of a network into an aggregated “external area” and a “study area” [16] and require the inclusion of currents as state variables [17]. Additionally, to the best of our knowledge, no low-order model exists to specifically compute nodal voltage and frequency for *all GFM nodes* in large-scale power systems.

This work advances the field by using physics-based reduction methods to develop low-order, accurate models for

frequency *and voltage dynamics* in all-inverter systems. GFM devices are modeled explicitly, while GLF inverters are modeled as negative load. The models are accurate and scalable, effectively eliminating the need for EMT simulations for a variety of applications. To this end, we first demonstrate the critical role of reactive power losses post-disturbance and its effect on voltage response and present novel methods for calculating post-disturbance reactive power participation factors for each GFM in a system. We then derive our proposed analytical models for frequency and voltage response for all-inverter systems. We utilize matrix exponentials to dramatically accelerate computation time. Using EMT simulation, we demonstrate the significant advantages that our models present with regards to solution speed and scalability, while preserving high accuracy. For these reasons, the models lend themselves well to direct application within industry and research environments. The ability to accurately and efficiently simulate transients in all-inverter systems sets the basis for probabilistic analysis of frequency and voltage stability as well as security-constrained economic dispatch and real-time dynamic security assessment, among other potential future applications.

I. THE NEED FOR NEW ANALYTICAL MODELS

In this section, we argue that the need for new analytical models of system dynamics is threefold. First, existing frequency response models are for 100% SG systems, or systems that are dominated by SGs, and are therefore intrinsically inappropriate for modeling all-inverter systems. Secondly, existing system frequency models neglect the heterogeneity of frequency response and the impacts of the transmission network, which we will demonstrate is particularly unsuitable for low-inertia, all-inverter systems. Finally, while existing models capture P- δ dynamics reasonably well, they assume Q- δ dynamics are insignificant, and as a result, voltage profiles are assumed to be 1 pu, which is only realistic for a network with large SGs. Hence, there is need for an analytical model that reflect this non-negligible coupling between active power and voltage, especially in all-inverter systems where these dynamics are even more critical [18]. In what follows, we discuss each of the above-mentioned issues in detail and present evidence in support of our arguments.

A. Frequency response: SG vs. GFM

The frequency response of all inverter systems is markedly different from that of conventional systems, where SGs provide frequency response. This difference arises from the fundamentally different way power and frequency are generated by GFMs vs. SGs. The frequency dynamics in SGs are initially governed by the mechanical momentum of the turbine, which determines the rate at which frequency deviates. This “inertial phase” is followed by primary frequency control, where the action of the turbine governor changes the generator’s active power output to arrest the frequency deviation [19]. The rate of change of frequency is entirely dependent on the generator momentum [18], commonly expressed in seconds and referred

to as the inertia constant. In primary frequency control, active power output changes as a function of the speed-droop coefficient, which is typically 5% [19]. Accordingly, the amount of momentum in the system and the governor response of the online generators collectively determine the frequency nadir, which is the point on the frequency response curve where frequency is lowest [11]. The frequency response mechanism of a generic SG is shown in Fig. 1.

While Newtonian physics guides frequency deviations in SGs, forming a second-order dynamical system, the frequency response of inverters is purely a function of their control algorithms; thus, as shown in [20], it presents a first-order dynamical system on the same timescales. There are three prominent control regimes for GFM including linear droop, virtual synchronous machines, and virtual oscillator control [20]. In this paper, we focus on multi-loop droop-control GFM (Fig. 1), due to their popularity and markedly different response shape as compared to SGs. In a droop control GFM, frequency is adjusted according to the device’s droop gain constant, which can be changed and is not intrinsic to the device [20]. Due to their very small inertia constant, lower nadirs are often observed in power systems with high shares of inverters [15], which is undesirable due to the legacy protection systems [21]. High RoCoF and low nadir values could unintentionally activate protection mechanisms, resulting in load-shedding. This was exactly the case in Britain on August 9th, 2019, when the Low Frequency Demand Disconnection (LFDD) protection mechanism was activated, tripping off massive amounts of distributed generation [22]. Therefore, it is important to develop computationally efficient analytical models that adequately capture frequency response in large systems with high shares of GFMs.

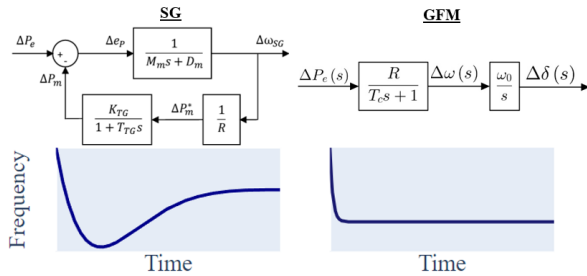


Fig. 1: Frequency response block diagram and response shape for: 1) SGs (left) and 2) GFMs (right) [23].

B. Network frequency heterogeneity

Many system frequency models are founded upon the operating principles of SGs and on the assumption of frequency being homogeneous across the network. Under this assumption, a system frequency model can be formulated by conveniently aggregating the parameters of SGs and modeling them as a single representative generator [6]. In such a model, there is no need to model how the generators in the system synchronize with each other and the impact of network topology is neglected. In reality, frequency is not

homogeneous across a power network. Rather, disturbance propagation – and therefore frequency response – is closely related to network topology. More specifically, disturbances are more severe in areas supporting the Fiedler eigenvalue of the network Laplacian [24]. Therefore, by aggregating generator parameters to approximate a “system frequency response,” one is ignoring the impact of network connectivity and systematically underestimating the maximum RoCoF and frequency deviation. To illustrate this effect, we simulate the outage of the Palo Verde Nuclear Generating Station in the WECC system, and the results are provided in Fig. 2.

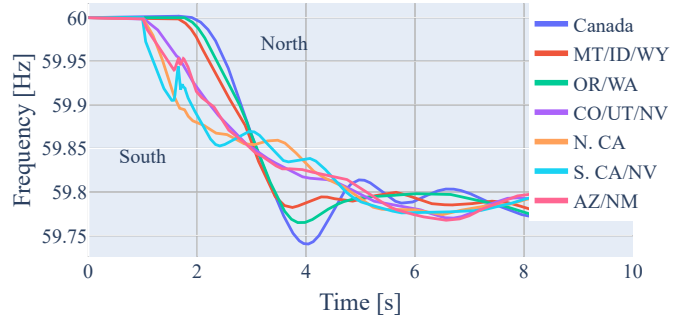


Fig. 2: PowerWorld simulation results of the WECC system following the outage of the Palo Verde Nuclear Generating Station, the system dimensioning contingency.

In Fig. 2, it is evident that even in this primarily SG network the frequency dynamics are not homogeneous, with varying values of RoCoF and nadir in each region. This suggests that neglecting the spatial-temporal characteristics of frequency response in a system yields inaccurate estimations of key metrics, particularly for large systems. Heterogeneity in frequency response could be exacerbated by higher shares of IBRs and a lack of inertia, leading to the simultaneous occurrence of frequency, voltage, and network dynamics [18]. Additionally, there is clearly a time delay between when significant deviation from nominal frequency begins to occur in the southern region versus in the northern region. Time delays between frequency response trajectories is another example of detail that is lost when representing the frequency response of a system with a single trajectory.

C. Voltage response and reactive power flow

While active power is the part of apparent power that does the work, reactive power is vitally important for preventing the demagnetization of transmission lines and sustaining voltages during transients [18]. Without adequate reactive power provision, low voltages may occur and contribute to a blackout [25]. The changing nature of frequency in IBR-dominated power systems also has ramifications in terms of voltage dynamics. While active and reactive power are closely related, frequency and voltage are treated independently in the conventional wisdom of power system analysis [19]. This is because in a conventional power system dominated by SGs, automatic voltage regulators (AVRs) locally control the

terminal voltage of SGs by adjustment of their field currents [19]. Because AVR dynamics are electromagnetic in nature, voltage regulation happens at a much faster timescale than frequency response, which is an electromechanical process in a SG dominated environment. Therefore, frequency and voltage dynamics are evaluated separately [18]. Due to the long-standing and ubiquitous treatment of voltage and frequency as decoupled, knowledge about the limits of the validity of the decoupling approach is lacking. At the same time, there is more need than ever to build upon our understanding of P-V and Q- δ dynamics due to new challenges posed by the introduction of IBRs. Unlike SGs, where frequency and voltage dynamics occur on different timescales, the frequency and voltage response of IBRs are both electromagnetic in nature [26]. The contemporaneousness of these dynamics may result in unexpected coupling dynamics and may lead to instabilities and low security [26]. Also distinguishing IBR dynamics from SG dynamics are constraints related to the silicon-based switches of power electronics. To avoid damaging these switches, IBRs limit their active and reactive power injections, whereas the power output of SGs is not bounded to the same degree; they can temporarily deviate from the excitation setpoint and supply a transient response which greatly exceeds the nominal rating of the machine [27]. In other words, while SGs are capable of providing generous active and reactive power during transients to support voltage and frequency, IBRs must more carefully provide power as to not violate current limits. As a result, the active and reactive power outputs of an IBR are closely related [18]. Here, we demonstrate the increased coupling in emergent power networks with all GFMs and the need to include both active and reactive power distribution factors.

Estimating Q-V dynamics post-disturbance is difficult due to the nonlinear nature of reactive power flow [28]. Interestingly, active power participation factors can still be reasonably estimated while neglecting Q-V dynamics, and [6]–[14] leverage this fact. To demonstrate this point, we simulate two different load steps in the IEEE 9-bus system and calculate the active and reactive power participation factors of each generator. The system has 3 GFM inverters and 3 constant power loads. Assuming generators have adequate headroom, we assert that the active and reactive participation factors of each generator can be estimated by solving the nonlinear power flow equations following a disturbance. The participation factors are equal to the change in power injection pre- and post-disturbance at each generation node. The calculation differs from the standard AC power flow because, instead of buses being categorized as $V\theta$ (slack), PV , and PQ types, they are only $V\theta$ and PQ type. Buses with GFMs are treated as $V\theta$ buses immediately after a disturbance and before the inverter controls have time to adjust their voltage angle and magnitude setpoints in response to changes in tie-in active and reactive power.

First, an active power load step of 31.5 MW is applied to Bus 6 and the active power participation factors are calculated. Then, a load step of 31.5 MW plus 9 MVar was applied to Bus 6, and again the active power participation factors are

calculated. Note that 31.5 MW is 10% of the active power load and 9 MVar is 10% of the reactive power load. The results, which are shown in Table I, indicate that even when a 10% reactive power load step is applied, the active power participation factors do not differ greatly.

TABLE I: Percent difference change in active power injection at generation buses, ΔP_G , between: 1) an active power load step, 2) an active and reactive power load step.

	Bus 1	Bus 2	Bus 3
% Difference ΔP_G	0.4612	0.9597	0.6341

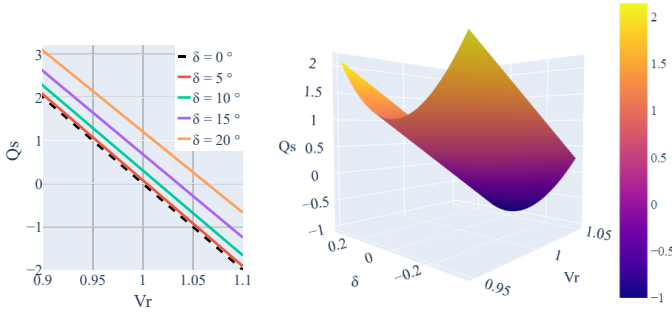
The picture is very different for changes in reactive power injection following a complex power disturbance. In Table II the results of participation factor calculations following seven disturbances are shown. In each of these simulations, a reactive power disturbance of 9 MVAR was applied to Bus 6. An active power step ranging from 0 MW to 30 MW was also applied in each simulation. The baseline ΔQ_G values were calculated following a 9 MVAR load step. Even though the magnitude of the reactive power load step was the same for each simulation, the reactive power injection at each generation node increases with the magnitude of the active power disturbance. For example, ΔQ_G at Bus 1 was 12.13% greater than the baseline value following the addition of a 5 MW load step. To explain this behavior, recall the equation for reactive power at the sending end of a transmission line (1) [19].

TABLE II: Percent difference in reactive power injection at generation buses, ΔQ_G , after complex load steps with increasing active power disturbance magnitudes.

% Error in ΔQ_G	Active Power Disturbance Magnitude [MW]						
	0	5	10	15	20	25	30
Bus 1	0	12.13	24.77	37.92	51.57	65.75	80.44
Bus 2	0	16.75	34.01	51.78	70.06	88.87	108.21
Bus 3	0	13.26	27.02	41.29	56.08	71.38	87.21

$$Q_S = \Im\{V_S I_S^*\} \approx \frac{V_S}{X} (V_S - V_R \cos \delta_{SR}) \quad (1)$$

Usually, δ_{SR} is assumed to be small and $\cos(\delta_{SR}) \approx 1$. This yields the trace corresponding to $\delta = 0^\circ$ in Fig. 3a [19], which is shown as a dashed line. After a disturbance, however, the angle across a transmission line δ_{SR} may increase, impacting reactive power injections across the system. If we choose not to approximate $\cos(\delta_{SR}) \approx 1$, we have a more complete picture of reactive power dynamics, as shown in Fig. 3. From this figure, we see there is significant curvature along the δ_{SR} axis, which illustrates there is a non-negligible relationship between voltage angle and reactive power. While Q- δ coupling is ignored in some studies [29], other works have attempted to account for this behavior. In [30] and [31], Q- δ dynamics are acknowledged but it is assumed that the slack bus alone changes its power injection to account for generation/load active power imbalances. In reality, all online generators will respond to the changes in states seen at their point of interconnection and therefore this assumption should not be



(a) Q_S vs. V_R for different values of δ_{SR} . (b) Sending-end reactive power as V_R and δ_{SR} change.

Fig. 3: Sending-end reactive power with respect to δ_{SR} and receiving-end voltage. $V_S = 1.0$ and $X = 0.05$.

made when attempting to estimate post-disturbance reactive power flow. In this paper, we improve upon previous efforts to estimate post-disturbance reactive power injections by distributing increased active power imbalances more realistically.

In summary, we established that the frequency transients across a power network could vary significantly due to individual generator properties, the fast nature of IBR frequency response mechanisms, and the impact of the transmission network. This frequency heterogeneity is especially pronounced in power networks with high shares of inverters. Moreover, to the author's knowledge, no low-order voltage response model has been developed for either SG-dominated or IBR-dominated systems. This constitutes a massive gap in our ability to estimate post-disturbance dynamics. There is an even greater need for models of Q-V dynamics post-disturbance seeing that the increased deployment of IBRs can give rise to weak grid conditions and compromise voltage stability [32]. These gaps in knowledge serve as the motivation to develop our frequency and voltage models for all-inverter systems, which will be discussed in the next section.

II. PROPOSED MODELS

In Section I-C we demonstrate how Q-V dynamics have a limited effect on active power participation factors and frequency. Conversely, changes in voltage angle have a non-negligible effect on the reactive power participation of each generator. Therefore, one can estimate frequency well without accounting for reactive power, but cannot estimate reactive power well without accounting for changes in phase angle. Given this information, we propose a frequency response model for all-inverter power systems that assumes decoupled dynamics, and a voltage response model that accounts for Q- δ dynamics. These models can be solved independently.

A. Frequency Response Model

The reduced-order block diagram representing the frequency response of a multi-loop droop GFM is shown in Fig. 1. The power error is detected through a low pass filter, creating a power error signal. This error signal serves as the input to the droop controller [23]. T_c is the reciprocal of the cut-off

frequency in Hz and R is the droop gain. The corresponding linearized equations are (2) and (3).

$$\Delta \dot{\delta} = \omega_0 \Delta \omega \quad (2)$$

$$\Delta \dot{\omega} = \frac{1}{T_c} (R \cdot \Delta P_e - \Delta \omega) \quad (3)$$

where δ is voltage angle, ω is frequency, and $\omega_0 = 2\pi * f_0$, where f_0 is the nominal network frequency, e.g. 60 Hz in the United States. The dot is the time derivative operator and Δ is the linear operator. Real and reactive nodal power injections are nonlinear functions of voltage magnitude and angle. These functions are typically linearized for a particular operating point [19]. Our frequency response model utilizes DC power flow approximations. These approximations yield the following network equations for active power.

$$P_k = \sum_{j=1, j \neq k}^N (B_{kj}(\theta_k - \theta_j)) \quad (4)$$

In the DC formulation, reactive power flow is disregarded because it is smaller than active power flow. The resulting linearized equation for power is (5), which can be written in terms of power injections at generation and load nodes as seen in (6). Grid-following inverters without grid support functionality may be treated as load nodes.

$$\Delta \mathbf{P} = \mathbf{B} \Delta \theta \quad (5)$$

$$\begin{bmatrix} \Delta P_G \\ \Delta P_L \end{bmatrix} = \begin{bmatrix} B_{GG} & B_{GL} \\ B_{LG} & B_{LL} \end{bmatrix} \begin{bmatrix} \Delta \theta_G \\ \Delta \theta_L \end{bmatrix} \quad (6)$$

The network is topologically reduced through the elimination of non-generator nodes [19], as follows:

$$\Delta \mathbf{P}_G = \underbrace{\mathbf{B}_{\text{red}} \Delta \theta_G}_{\Delta \mathbf{P}_{os}} + \underbrace{\mathbf{B}_L \Delta \mathbf{P}_L}_{\Delta \mathbf{P}_d} \quad (7)$$

where $\mathbf{B}_{\text{red}} = \mathbf{B}_{GG} - \mathbf{B}_{GL} \mathbf{B}_{LL}^{-1} \mathbf{B}_{LG}$ and $\mathbf{B}_L = \mathbf{B}_{GL} \mathbf{B}_{LL}^{-1}$. From (7) we see that the change in power at a generation node is a function of the differences in angles between generation nodes and the change in power injections at the non-generator nodes [14]. We refer to the first term of (7) as the inter-machine oscillation of power. The second term, which is denoted as $\Delta \mathbf{P}_d$ is interpreted as the change in power injections at generation nodes due to a disturbance. $\Delta \mathbf{P}_d$ is a vector with a number of elements equal to the number of generators. $\Delta \mathbf{P}_L$ is the vector of load changes. For instance, consider a system with three load buses and a load step at load bus 3. The third element of $\Delta \mathbf{P}_L$ is then $P_{step} * K_l$, where K_l is the approximated marginal loss constant. Average transmission and distribution losses are about 2-5%, and therefore we recommend choosing 1.05 as the value of K_l to avoid overestimating nadir and settling frequency [33]. The higher the value of K_l , the more conservative the estimate of nadir and settling frequency. For a system with N_G droop control GFMs, there will be $2N_G - 1$ first-order differential equations

which are shown in compact state-space form in (8). Note $\alpha_i = \frac{S_B}{S_i}$ and $\omega_0 = 2\pi f_0$ where $f_0 = 60$ in the United States.

$$\begin{bmatrix} \Delta \dot{\delta}_{i,n-1} \\ \Delta \dot{\omega}_i \end{bmatrix} = \underbrace{\begin{bmatrix} \mathbf{0} & \mathbf{1}_{-1} \\ \mathbf{B}_n & \mathbf{T}_n \end{bmatrix}}_{\mathbf{A}_f} \begin{bmatrix} \Delta \delta_{i,n-1} \\ \Delta \omega_i \end{bmatrix} + \underbrace{\begin{bmatrix} \mathbf{0} \\ \gamma_n \end{bmatrix}}_{\mathbf{B}_f} [\Delta P_d] \quad (8)$$

where

$$\mathbf{B}_n = -diag\left(\frac{\omega_0 \alpha_n R_n}{T_{cn}}\right) \mathbf{B}'_{red}, \quad \mathbf{T}_n = -diag\left(\frac{1}{T_{cn}}\right) \quad (9)$$

$$\gamma_n = diag\left(\frac{\omega_0 \alpha_n R_n}{T_{cn}}\right)$$

The angles in (8) are relative angles $\Delta \delta_{1n} \dots \Delta \delta_{n-1,n}$ and \mathbf{B}'_{red} is equal to \mathbf{B}_{red} with the n^{th} column removed. We refer to the proposed frequency response model as the Low-Inertia Frequency Evolution (LIFE) model.

B. Voltage Response Model

The LIFE model made the standard assumption of decoupled active and reactive power flow. Here, we propose a model of voltage response that accounts for post-disturbance Q- δ coupling and can be thought of as the counterpart of our frequency response model. The reduced-order block diagram representing the reactive power droop of a multi-loop GFM is given in Fig. 4. M_q is the reactive power droop value.

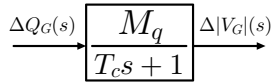


Fig. 4: Low-order model of reactive droop.

Given that reactive power cannot travel long distances and voltage magnitudes do not synchronize across a network, the open loop model of Fig. 4 is a reasonable method for estimating voltage response locally [19]. The model must be provided with a good approximation of the change in reactive power injection at the generator nodes, ΔQ_G . The equation for instantaneous reactive power injection is (10).

$$Q_i = - \sum_{j=1}^n B_{ij} V_i V_j \cos(\theta_{ij}) + \sum_{j=1}^n G_{ij} V_i V_j \sin(\theta_{ij}) \quad (10)$$

Assuming the reactive power set points of all GFMs are known, the change in reactive power injection due to the disturbance can be described as (11).

$$\Delta Q_G = Q_G(V_{post}, \theta_{post}) - Q_{G0} \quad (11)$$

where V_{post} and θ_{post} are the post-disturbance angles and voltages, and Q_{G0} is the inverter Q set point. We propose the following steps for estimating $Q_G(V_{post}, \theta_{post})$ and ΔQ_G .

- 1) Estimate each new GFM active power injection using $P_{Gi}(V_{post}, \theta_{post}) \approx \Delta P_{di} + P_{Gi0}$ where ΔP_{di} is calculated in (7).
- 2) In the AC power flow formulation, update the active power injections to reflect $P_{Gi}(V_{post}, \theta_{post})$, ΔP_L , and ΔQ_L . Then solve AC power flow.

- 3) The updated Q values are approximately equal to $Q_G(V_{post}, \theta_{post})$.
- 4) Approximate ΔQ_G using (11).

The difference between solving for $Q_G(V_{post}, \theta_{post})$ as described in Section I-C and in the process enumerated above boils down to the assumed known quantities at each generator bus. In a classic AC power flow problem, P and V are the known quantities at the generation buses, while in the proposed formulation of Section I-C, V and θ are the known quantities. However, since P and θ are closely related, these approaches yield nearly identical results, as shown in Table III. The benefit of using the process enumerated above is that it allows for the leveraging of AC power flow solvers, which are ubiquitous and effective for large systems.

TABLE III: Validation of proposed reactive power injection approximation method.

	Bus 1	Bus 2	Bus 3
% Error of ΔQ_G	0.2947	0.7333	0.2789

In a droop-controlled GFM, the quadrature-axis (q-axis) voltage is adjusted according to the droop value M_q and the change in reactive power injection ΔQ_G [34]. This adjusted q-axis voltage then passes through the voltage controller and current controller before the q-axis and direct-axis (d-axis) voltages are transformed into the phase voltages V_a , V_b , and V_c via the inverse Park Transformation. These voltages serve as the inputs to the inverter LCL filter [34]. As a result, the change in voltage magnitude at the generator bus is actually several times larger than ΔV_G as calculated in (13). Therefore, to calculate the exact change in voltage magnitude at the generator bus would require modeling these additional controls and including the q-axis and d-axis currents and voltages. This would increase the number of states in the system several times over, which would severely diminish the computational tractability of the voltage response model for large systems, and thus defies the original purpose of reduced-order models. We propose the introduction of the voltage outer-loop-to-grid constant, K_v , to maintain computational efficiency for a voltage response model. This constant is specific to each inverter as it accounts for the aggregation of all coefficients involved, including the equivalent gain factor between the droop-adjusted V_q and the post voltage and current controller V_g , as well as the factor for conversion from phase-to-neutral to line-to-line voltage and conversion to RMS. Depending on the specific GFM inverter, this constant can vary. After extensive, computational experimentation with industry-grade models, we determine values between 3 and 6 are most appropriate for the models used in [34]. Fidelity could be gained through further tuning of this parameter for specific scenarios - here, we present the most general form. The change in voltage magnitude at a generator bus is approximated by (12), where $V_{G,grid}$ is the voltage at the terminal of the GFM. We subsequently refer to this model of voltage response, which is given in state-space form in (13), as the Low-Inertia Voltage Evolution (LIVE) model. In this formulation, B_v encodes the

settling voltage and A_v encodes the pace at which the settling voltage is reached.

$$\Delta V_{G,grid} \approx K_v \cdot \Delta V_G \quad (12)$$

$$[\Delta|\dot{V}_{G,grid}|] = \mathbf{A}_v [\Delta|V_{G,grid}|] + \mathbf{B}_v [\Delta Q_G] \quad (13)$$

where

$$\mathbf{A}_v = -diag\left(\frac{1}{T_{cn}}\right), \quad \mathbf{B}_v = diag\left(\frac{\alpha_n M_{qn} K_v}{T_{cn}}\right) \quad (14)$$

C. Computational Solver and Acceleration

For small and medium-sized systems, solving (8) using a solver such as ode45 in MATLAB provides fast results. However, this is inefficient for large systems. A superior solving method for large, linear time-invariant (LTI) state equations involves reformulating (8) as a discrete-time system using a matrix exponential as shown in (15) [35]. The closed form solution is then (16). Assuming the generator dispatch is known, matrices \mathbf{A}_f and \mathbf{B}_f can be converted into their discrete-time formulations offline. Then, the disturbance magnitude and location, which is encoded in the vector u , serves as the input to (16).

$$A_d = e^{AT_s}, \quad B_d = (A_d - I)BA^{-1} \quad (15)$$

$$x[k+1] = A_d x[k] + B_d u[k] \quad (16)$$

D. Implementation and Workflow

The suggested workflow for the implementation of the LIFE and LIVE models is shown in Fig. 5. The susceptance matrix, \mathbf{B} can be obtained from the MATPOWER, PowerWorld, TSAT, PSSE, or PSLF file of the relevant system for offline applications (planning case) and directly exported from the state estimator for online applications (operations case). The generator dispatches are determined by power flow calculations if conducting multi-scenario offline dynamics studies and directly by the state estimator if conducting online dynamic assessment. Next, for a given generator dispatch, \mathbf{A}_f , \mathbf{B}_f , \mathbf{A}_v , and \mathbf{B}_v are calculated and converted to discrete-time. The computations in discrete-time are exceptionally fast, making it suitable to run on most commonly available computers for operational applications or real-time contingency screening.

III. COMPUTER SIMULATION AND VALIDATION

We used the WSCC 9-bus system and IEEE 39-bus system benchmarks to test and verify the accuracy of the frequency response model given in (8) against industry-grade standard EMT simulations. The WSCC 9-bus model was constructed in PSCAD and utilizes the inverter models from [34], which are quite complex and validated against real-world data from the Maui power systems. In this system, all GFMs have a rated capacity of 200 MVA, an active power droop constant of 5%, and a power measurement time constant of 0.0628 seconds. A 31.5 MW + 9 MVAR load step at Bus 6 was simulated. A marginal loss constant of 1.035 is assumed. Visual inspection of the results indicate that the data from PSCAD verifies the accuracy of the LIFE model, as shown in Fig. 6. The runtimes

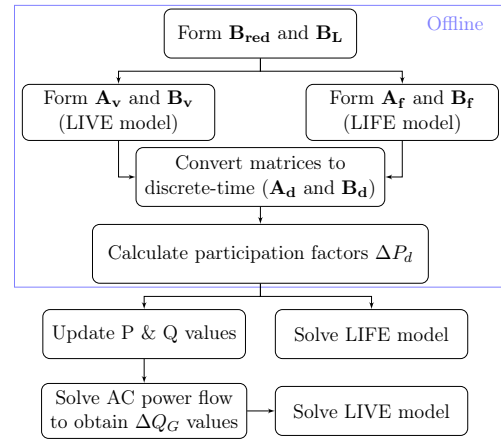


Fig. 5: Workflow for the LIFE and LIVE models. The disturbance magnitude is embedded into ΔP_d as indicated in (7).

to obtain five seconds of simulation data are given in Table IV. To further demonstrate the computational advantage of our method, we also ran another version of the WSCC 9-bus system in PowerWorld and used the REGFM_A1 model [36]. The proposed model has the benefit of significantly accelerated solve time. While this is a small test case, computational accelerations of $\approx 250x$ over EMT simulations and $\approx 100x$ over RMS simulations create incredible opportunities for online operational applications.

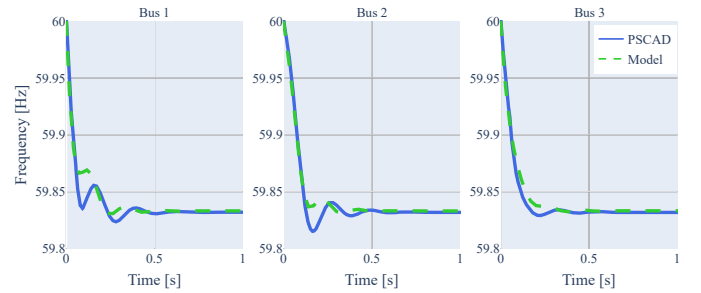


Fig. 6: LIFE vs. PSCAD simulations in the 9-bus system.

TABLE IV: Simulation runtime comparison of the WSCC 9 bus network.

	PSCAD	PowerWorld	LIFE Model
Runtime (sec)	16,594	6,094	0.006
Acceleration factor	264	97	n/a

The LIFE model was also validated against the 39 Bus system following a 307.5 MW + 141 MVAR load step at Bus 15. We observe good agreement between the LIFE model and the simulated trajectories, as shown in Fig. 7. In addition to nadir and RoCoF, we use the hertz-sec (HS) metric, which is a proxy for the kinetic energy resulting from a disturbance, to evaluate the accuracy of the LIFE model. The HS metric integrates the absolute value of frequency deviation over the transient period, as shown by the shaded area in Fig. 7b. It is calculated using $HS = \int_{t_0}^{t_s} |f_0 - f(t)| dt$, where t_0 and t_s

are the time transient behavior begins and the time settling frequency is reached, respectively [23]. The pre-disturbance frequency is f_0 and the transient frequency is a function of time, $f(t)$. In Table V, the error of nadir, RoCoF, and HS calculated using the LIFE model are given. While error of these key metrics was small, the required accuracy will be application-specific.

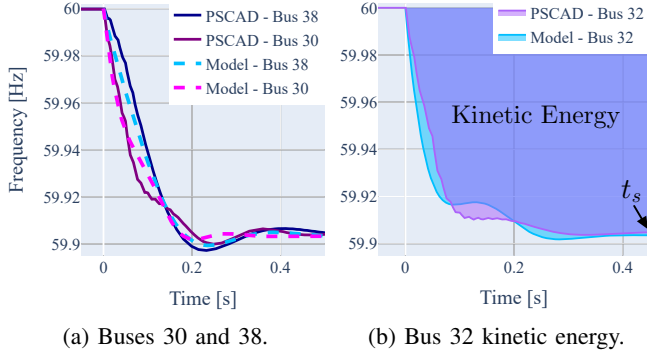


Fig. 7: LIFE vs. PSCAD results in the 39-bus system. The HS metric is a proxy for kinetic energy.

TABLE V: |Error| of key metrics in the 39-bus system: LIFE vs. PSCAD.

	Nadir [Hz]	RoCoF [Hz/s]	HS [Hz·s]
Bus 30	0.0079	0.0518	0.0006
Bus 31	0.0042	0.2420	0.0002
Bus 32	0.0041	0.3504	0.0003
Bus 33	0.0046	0.2915	0.0004
Bus 34	0.0088	0.2693	0.0001
Bus 35	0.0048	0.3523	0.0006
Bus 36	0.0068	0.3790	0.0006
Bus 37	0.0075	0.1668	0.0003
Bus 38	0.0106	0.2381	0.0000
Bus 39	0.0088	0.0712	0.0009
Average	0.0068	0.2412	0.0004

Next, we validate the LIFE model against the same simulation scenarios (10% complex load step) used to generate the traces in Figs. 6 and 7. A K_v value of 5 was used for both the 9 and 39 bus system. The results, shown in Table VI, Fig. 8, and Table VII point to the effectiveness of this approach. The PSCAD voltage traces in Fig. 8 indicate negligible voltage oscillations, and therefore voltage transients are well approximated by a first order model without feedback. The lack of oscillation in the voltage magnitudes confirms that local changes in voltage magnitude and reactive power do not propagate well, and have a negligible effect on voltage magnitude at surrounding generator buses. While the inner-loop controls and LCL filter have an effect on the change in voltage magnitude at the generator bus, reasonable estimates of ΔQ_G and K_v provide good approximations of voltage response without the need for explicit modeling of inner-loop controls. The validity of this approach is supported by the exceedingly small average error of settling voltage, which was just 0.0019 pu in the 9 bus system and 0.0021 pu in the 39

bus system. In the 39 bus system, the largest change in voltage magnitude was -0.011 pu, which occurred at Bus 35.

TABLE VI: Settling voltage error [pu] in the 9-bus system: LIVE model vs. PSCAD simulations.

	Bus 1	Bus 2	Bus 3
Error [pu]	0.0001	0.0043	0.0015

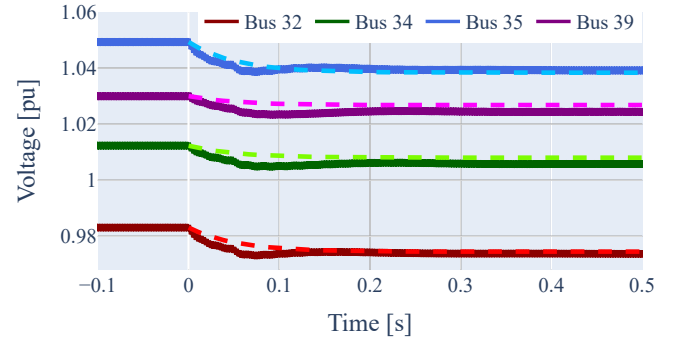


Fig. 8: LIVE (dashed lines) vs. PSCAD simulations (solid lines) in the IEEE 39 bus system.

TABLE VII: Settling voltage error [pu] in the 39-bus system: LIVE model vs. PSCAD simulations.

	Bus 30	Bus 31	Bus 32	Bus 33	Bus 34	Bus 35
Error [pu]	0.0021	0.0012	0.0014	0.0009	0.0029	0.0003
	Bus 36	Bus 37	Bus 38	Bus 39		
Error [pu]	0.0030	0.0032	0.0045	0.0014		

IV. SCALABILITY AND APPLICATION: 25,000-BUS SYSTEM

Having demonstrated the efficacy of our models in the previous section, we now focus on their scalability and application to large-scale systems. The frequency response and voltage response models were applied to the open-source ACTIVSg25k synthetic grid of the northeastern United States [37], which is shown in Fig. 9. This is an extremely large system, comprising most of three independent system operators' territories, with additional vertically integrated utility territory included. For every bus with multiple generators, we aggregated generators into one generator with an equivalent capacity. We then converted all the generators with capacities exceeding 100 MVAR to be droop-controlled GFMs. This resulted in 849 GFM buses. The remaining 24,151 buses are modeled as load buses in (6). All generators below this capacity were considered GFLs and modeled as negative load. A very large system formed entirely by GFMs is an exaggerated version of potential future power systems. We utilize the frequency and voltage models on such a system to demonstrate their efficiency on systems where EMT simulation would be impossible and computational efficiency is paramount. A 1.56 GW + 780 MVAR load step was applied to Bus 69665 in New York City. The active power disturbance magnitude is equal to the capacity of the largest online generator, and the

reactive power disturbance magnitude is equal to half of the active power disturbance magnitude. The active-droop constant and power measurement time constant of each inverter were 5% and 0.0628 seconds, respectively. A T_s value of 0.001 was used and (16) was solved in only 13.004 seconds to obtain 1 second worth of simulated frequency response, which is sufficient given the faster response of GFM compared to SGs. To illustrate the heterogeneity of frequency response, the predicted frequency response in five different areas across the system are shown in Fig. 10. The frequency trajectories for all GFM buses are also shown. The results indicate that while all frequencies in the system synchronize within a second, GFM buses closest to the disturbance experience dramatic frequency oscillations and more distant buses display much smoother trajectories. This behavior is expected, seeing as GFM buses closest to a disturbance will be subjected to greater changes in active power injection, according to (7). Also noteworthy is the time delay between the onset of transients between areas close to the disturbance versus areas farther from the disturbance. This is perhaps most obvious when comparing the frequency trajectories in New York City to those in South Carolina, where frequency deviation is delayed by about .18 seconds.

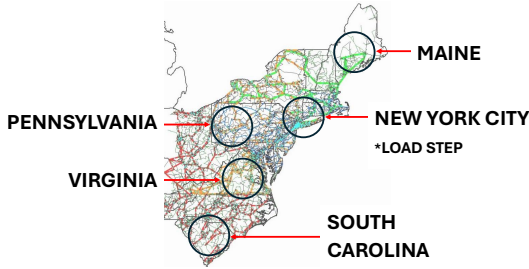


Fig. 9: 25k bus synthetic grid of the northeastern United States [37]. A load step was applied in New York City, and frequency was observed in five regions across the network.

Fig. 11 depicts the box plots of the LIFE nadir and RoCoF values in the ACTIVSg25k network post-disturbance. The LIFE model captures the spatial and temporal differences in frequency response as these variations in frequency could mean the difference between protection mechanisms tripping or not. Therefore, the model’s ability to capture frequency response extrema is exceedingly important. In this scenario, the average frequency nadir was 59.96 Hz and the average RoCoF was 1.30 Hz/sec. Of the 849 GFM buses, 143 buses experienced RoCoFs exceeding 1 Hz/sec and the maximum RoCoF was a staggering 113.6 Hz/sec. As expected, the largest RoCoF values were seen at buses closest to the disturbance and at buses with small GFM capacities. Even so, the nadir frequency at these buses is about 59.77 Hz, which does not violate the underfrequency load shedding limit [38].

The voltage response model solved in just 0.127 seconds due to the approximation of Q-V dynamics as an open-loop process. K_v was set equal to 5. As seen in Fig. 11, most GFM buses experienced negligible changes in reactive power injection and voltage magnitude, with a few crucial exceptions.

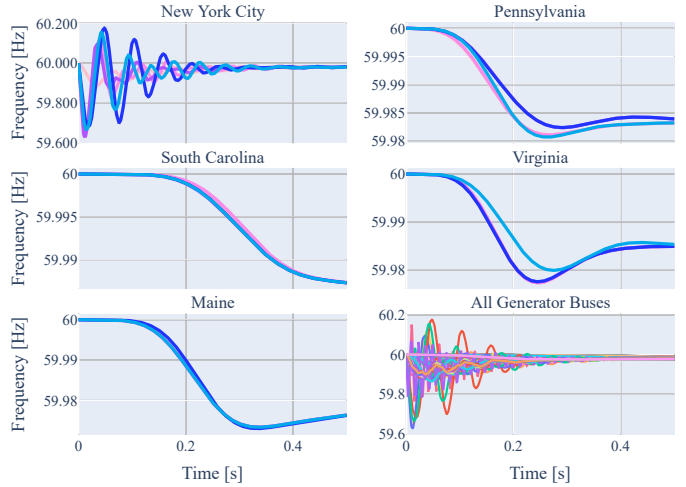


Fig. 10: Predicted frequency response in five regions across the ACTIVSg25k network. Frequency traces at all 849 GFM buses are shown in the bottom right corner. All frequencies reached a stable value of 59.98 ± 0.005 Hz after 0.589 seconds.

The average change in voltage magnitude was 0.0009 pu and the maximum was 0.19 pu. The predicted voltage trajectories at GFM buses where $\Delta V > 0.01$ pu are shown in Fig. 12. The greatest changes in reactive power injection and voltage variations are seen at the generators electrically closest to the load step location, which makes sense given the limited range of reactive power disturbances. There were four GFM buses at which reactive power deficiency caused the voltage magnitude to settle below 0.95 pu.

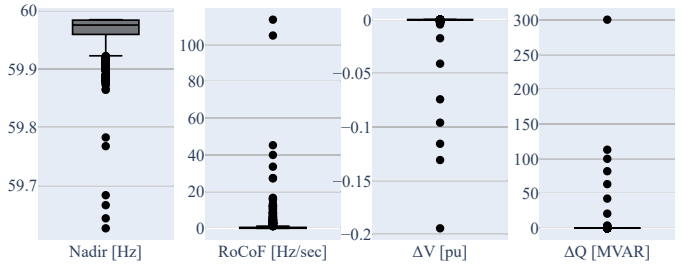


Fig. 11: Box plots of nadir, absolute value of RoCoF, change in voltage magnitude, and change in reactive power injection at each GFM bus in the ACTIVSg25k test case.

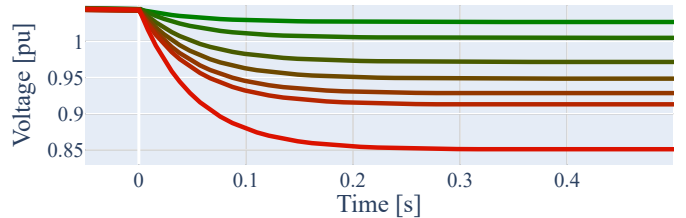


Fig. 12: Voltage trajectories at GFM buses where the change in voltage magnitude exceeded 0.01 pu.

V. CONCLUSION

While frequency response models have a history spanning decades, many models disregard the heterogeneity of the frequency response and assume that the network is dominated by synchronous generators. All disregard reactive power-voltage dynamics. In this paper we present models of frequency and voltage response for 100% IBR networks. The models were validated on the WSCC 9 bus and IEEE 39 bus systems. The models were then utilized to predict frequency and voltage response in a 25,000 bus synthetic system. Our results indicate that the models provide reasonable estimations of frequency and voltage response at every GFM bus in the system while, crucially, maintaining computational tractability, setting the basis for their use in planning and operational applications.

REFERENCES

- [1] Executive summary – Renewables 2023 – Analysis. IEA. [Online]. Available: <https://www.iea.org/reports/renewables-2023/executive-summary>
- [2] R. W. Kenyon, B. Wang, A. Hoke, J. Tan, C. Antonio, and B.-M. Hodge, “Validation of Maui PSCAD Model: Motivation, Methodology, and Lessons Learned,” in *2020 52nd North American Power Symposium (NAPS)*. IEEE, pp. 1–6.
- [3] S. Zhu, D. Piper, D. Ramasubramanian, R. D. Quint, A. Isaacs, and R. Bauer, “Modeling inverter-based resources in stability studies,” *2018 IEEE Power & Energy Society General Meeting (PESGM)*, pp. 1–5, 2018.
- [4] J. G. Simmonds and J. E. Mann, *A First Look at Perturbation Theory*, 2nd ed. Dover.
- [5] P. Kokotovic and P. Sauer, “Integral manifold as a tool for reduced-order modeling of nonlinear systems: A synchronous machine case study,” *IEEE Transactions on Circuits and Systems*, vol. 36, no. 3, pp. 403–410, 1989.
- [6] M. Chan, R. Dunlop, and F. Schweppe, “Dynamic Equivalents for Average System Frequency Behavior Following Major Disturbances,” vol. PAS-91, no. 4, pp. 1637–1642.
- [7] P. Anderson and M. Mirheydar, “A low-order system frequency response model,” *IEEE Transactions on Power Systems*, vol. 5, no. 3, pp. 720–729, 1990.
- [8] D. L. H. Aik, “A general-order system frequency response model incorporating load shedding: analytic modeling and applications,” *IEEE Transactions on Power Systems*, vol. 21, no. 2, pp. 709–717, 2006.
- [9] Y. Zhang, Q. Guo, Y. Zhou, and H. Sun, “Frequency-constrained unit commitment for power systems with high renewable energy penetration,” vol. 153, p. 109274.
- [10] I. Egido, F. Fernandez-Bernal, P. Centeno, and L. Rouco, “Maximum frequency deviation calculation in small isolated power systems,” *IEEE Transactions on Power Systems*, vol. 24, no. 4, pp. 1731–1738, 2009.
- [11] L. Liu, W. Li, Y. Ba, J. Shen, C. Jin, and K. Wen, “An analytical model for frequency nadir prediction following a major disturbance,” *IEEE Transactions on Power Systems*, vol. 35, no. 4, pp. 2527–2536, 2020.
- [12] S. Yang, Q. Meng, Y. Zhang, Z. Hao, and B. Zhang, “Simplified prediction model of frequency nadir for power systems penetrated with renewable energy,” in *2022 IEEE Power & Energy Society General Meeting (PESGM)*, 2022, pp. 1–5.
- [13] S. Dong, X. Fang, J. Tan, N. Gao, X. Cui, and A. Hoke, “A Unified Analytical Method to Quantify Three Types of Fast Frequency Response from Inverter-based Resources.” [Online]. Available: <http://arxiv.org/abs/2209.09413>
- [14] X. Wang, W. Li, J. Shen, S. Zhao, and Q. Zhang, “A three-machine equivalent system frequency response model and its closed-form solution,” vol. 142, p. 108344.
- [15] Y. Lin, J. H. Eto, B. B. Johnson, J. D. Flicker, R. H. Lasseter, H. N. V. Pico, G.-S. Seo, B. J. Pierre, and A. Ellis, “Research Roadmap on Grid-Forming Inverters,” p. 60. [Online]. Available: <https://www.nrel.gov/docs/fy21osti/73476.pdf>
- [16] Y. Du, X. Lu, and D. Zhao, “Model reduction for inverter-dominated networked microgrids with grid-forming inverters,” in *IECON 2021 – 47th Annual Conference of the IEEE Industrial Electronics Society*, 2021, pp. 1–6.
- [17] O. Ajala, N. Baeckeland, B. Johnson, S. Dhople, and A. Domínguez-García, “Model reduction and dynamic aggregation of grid-forming inverter networks,” *IEEE Transactions on Power Systems*, vol. 38, no. 6, pp. 5475–5490, 2023.
- [18] A. Sajadi and B.-M. Hodge, “Plane Wave Dynamic Model of Electric Power Networks with High Shares of Inverter-Based Resources.”
- [19] J. Machowski, Z. Lubosny, and J. W. Bialek, *Power System Dynamics*.
- [20] R. W. Kenyon, A. Sajadi, M. Bossart, A. Hoke, and B.-M. Hodge, “Interactive power to frequency dynamics between grid-forming inverters and synchronous generators in power electronics-dominated power systems,” *IEEE Systems Journal*, vol. 17, no. 3, pp. 3456–3467, 2023.
- [21] A. Sajedi, L. Strezoski, A. Khodaei, K. Loparo, M. Fotuhi-Firuzabad, R. Preece, M. Yue, F. Ding, V. Levi, P. Arboleya, and V. Terzija, “Guest editorial: Special issue on recent advancements in electric power system planning with high-penetration of renewable energy resources and dynamic loads,” *International Journal of Electrical Power and Energy Systems*. [Online]. Available: <https://www.osti.gov/biblio/1769842>
- [22] “GB power system disruption on 9 August 2019.”
- [23] A. Sajadi, R. W. Kenyon, and B.-M. Hodge, “Synchronization in electric power networks with inherent heterogeneity up to 100% inverter-based renewable generation,” vol. 13, no. 1, p. 2490.
- [24] L. Pagnier and P. Jacquod, “Inertia location and slow network modes determine disturbance propagation in large-scale power grids,” vol. 14, no. 3, p. e0213550.
- [25] N. A. E. R. Council, *Technical Analysis of the August 14, 2003 Blackout: What Happened, Why, and What Did We Learn?* North American Electric Reliability Council.
- [26] F. Milano, F. Dörfler, G. Hug, D. J. Hill, and G. Verbič, “Foundations and challenges of low-inertia systems (invited paper),” in *2018 Power Systems Computation Conference (PSCC)*, 2018, pp. 1–25.
- [27] R. W. Kenyon, A. Hoke, J. Tan, and B.-M. Hodge, “Grid-following inverters and synchronous condensers: A grid-forming pair?” in *2020 Clemson University Power Systems Conference (PSC)*, 2020, pp. 1–7.
- [28] B. Gentile, J. W. Simpson-Porco, F. Dörfler, S. Zampieri, and F. Bullo, “On reactive power flow and voltage stability in microgrids,” in *2014 American Control Conference*, 2014, pp. 759–764.
- [29] M. Ilic-Spong and A. Phadke, “Redistribution of reactive power flow in contingency studies,” *IEEE Transactions on Power Systems*, vol. 1, no. 3, pp. 266–274, 1986.
- [30] S. Singh and S. Srivastava, “Improved voltage and reactive power distribution factors for outage studies,” *IEEE Transactions on Power Systems*, vol. 12, no. 3, pp. 1085–1093, 1997.
- [31] P. A. Ruiz and P. W. Sauer, “Post-contingency voltage and reactive power estimation and large error detection,” in *2007 39th North American Power Symposium*, 2007, pp. 266–272.
- [32] M. G. Dozein, P. Mancarella, T. K. Saha, and R. Yan, “System Strength and Weak Grids: Fundamentals, Challenges, and Mitigation Strategies,” in *2018 Australasian Universities Power Engineering Conference (AUPEC)*, pp. 1–7.
- [33] Frequently Asked Questions (FAQs) - U.S. Energy Information Administration (EIA). [Online]. Available: <https://www.eia.gov/tools/faqs/faq.php>
- [34] R. W. Kenyon, A. Sajadi, A. Hoke, and B.-M. Hodge, “Open-Source PSCAD Grid-Following and Grid-Forming Inverters and A Benchmark for Zero-Inertia Power System Simulations,” in *2021 IEEE Kansas Power and Energy Conference (KPEC)*. IEEE, pp. 1–6.
- [35] R. C. Dorf and R. H. Bishop, *Modern Control Systems*, 12th ed. Prentice Hall, Pearson.
- [36] W. Du, Q. H. Nguyen, S. Wang, J. Kim, Y. Liu, S. Zhu, F. K. Tuffner, and Z. Huang, “Positive-sequence modeling of droop-controlled grid-forming inverters for transient stability simulation of transmission systems,” *IEEE Transactions on Power Delivery*, vol. 39, no. 3, pp. 1736–1748, 2024.
- [37] A. B. Birchfield, T. Xu, K. M. Gegner, K. S. Shetye, and T. J. Overbye, “Grid structural characteristics as validation criteria for synthetic networks,” *IEEE Transactions on Power Systems*, vol. 32, no. 4, pp. 3258–3265, 2017.
- [38] “Manual 33 System Protection Manual,” New York Independent System Operator.